An atomistic simulation of phase transitions and charge mobility for the organic semiconductor Ph-BTBT-C10

Alberto Baggioli,[†] Mosè Casalegno,[†] Guido Raos,[*,†] Luca Muccioli,[‡] Silvia Orlandi,[*,‡] and Claudio Zannoni[*,‡]

†*Department of Chemistry, Materials and Chemical Engineering "G. Natta", Politecnico di Milano, via L. Mancinelli 7, 20131 Milano, Italy*

‡*Dipartimento di Chimica Industriale "Toso Montanari", Università di Bologna, viale Risorgimento 4, 40136 Bologna,ITALY*

E-mail: guido.raos@polimi.it; s.orlandi@unibo.it; claudio.zannoni@unibo.it

Abstract

We present a computational study of the molecular organization and charge mobility of Ph-BTBT-C10, a high performance organic semiconductor of considerable current interest. We have observed for the first time by atomistic molecular dynamics the formation of an ordered smectic phase on cooling down from the isotropic melt and upon heating the crystal, for this system, in good agreement with experiment. Although we could observe only a smectic A and not a smectic E phase, the temperature variation of the hole mobility estimated from hopping model calculations reproduces the main features of experiments. The crystal phase is characterized by high mobility bilayers defined by the aromatic π-conjugated cores, but it is effectively insulating in the orthogonal direction. The smectic phase is characterized by more disordered monolayers, which have a good in-plane mobility and a lower, but still appreciable, degree of

charge transport across the layers. This feature may be advantageous for applications requiring materials with evenly balanced, three-dimensional conduction paths.

Keywords

Molecular Dynamics, Smectic phases, Kinetic Monte Carlo, Organic Semiconductors, BTBT

Introduction

Organic semiconductors (OSCs) comprise a vast array of molecules and polymers with a π-conjugated core. They are proving a valuable alternative to traditional inorganic ones in a variety of applications ranging from transistors to light-emitting diodes and solar cells.[1–3] These soft functional materials have a number of advantages, particularly for being amenable to solution processing, instead of vapor deposition, thus facilitating roll to roll industrial processes and in turn the fabrication of large area, light weight and flexible devices. However, one of the limiting factors of this technology has been the relative poor performance of OSCs, particularly because of their usually low charge mobility. This is not surprising since organic materials are typically insulators, with charge mobility of the order of 10^{-5} cm^{2}V^{-1}s^{-1}, even if the performance can be somehow improved by adding n or p molecular dopants,[4] but materials with good intrinsic semiconductor features also exist.[5]

The problem of optimizing the performance of OSCs is complicated by the fact that the relation between molecular features, morphologies and transport performance is still far from established. One of the key aspects is undoubtedly the phase organization of the molecules, e.g. amorphous or liquid crystalline or crystal in the various polymorphs, but there are also other factors such as the presence of trapping defects.[5] Given a certain material, the importance of morphology has been shown, e.g. in the classic work by Warman

on columnar triphenylene liquid crystals,[6] where the system is insulating in the isotropic phase and becomes a semiconductor when cooled down in the columnar phase, with a mobility increased by three orders of magnitude (from $\approx 10^{-4}$ to $\approx 10^{-1}$ $cm^2V^{-1}s^{-1}$). In π-conjugated materials at room temperature, the mobility mechanism is typically associated to charge hopping and regulated by Marcus theory,[7] to be discussed later. Brédas and coworkers have shown how charge transport is greatly affected by the magnitude of the electronic coupling between the pair of molecules involved in the hopping, that in turn depends on their relative molecular positions and orientations.[8,9] The literature offers several alternatives to this theory. Some of them are simpler but have a greater empirical content.[10] Others are rooted in more sophisticated quantum mechanical treatments of the coupled electron-nuclear dynamics, including tunnelling and delocalization effects,[11,12] but they are hardly applicable to the complex molecular morphologies produced by large, atomistic MD simulations such as those described here. Marcus hopping theory currently appears to be a convenient compromise between rigour and computational complexity.[13,14]

The role of the organic semiconductor processing in the fabrication of actual devices has also been the focus of many experimental investigations, with various attempts to achieve the appropriate molecular packing, e.g. using thermal gradients[15] or vapor assisted crystallization.[16] These techniques can influence performance in multiple ways, often (and sometimes fortuitously) yielding, via non-equilibrium processes, morphologies difficult to achieve via thermodynamic equilibrium routes. In general, order in the molecular organization is an important parameter for maximizing organic semiconductor performances, and in this respect materials exhibiting liquid crystal mesophases at equilibrium or in the course of non-equilibrium processing are of interest.[17–19] The existence of a liquid crystal phase arising during a spin-coating solvent evaporation process has, in particular, been deemed significant towards improving the OSC film quality and resulting performance.[20]

Recently, a family of small π-conjugated molecules based on a [1]benzothieno[3,2-

b]benzothiophene (BTBT) unit with symmetric or asymmetric lateral substitutions (see, for example Ph-BTBT-C10 in Fig. 1) have attracted great interest for their very high performance,[21–25] with mobilities of the order of 10 $cm^2V^{-1}s^{-1}$ or higher,[22,26,27] even in solution processed organic field effect transistors (OFET).[15,28,29] In addition to mobility itself, the integration of BTBT-based films into a robust transistor circuit technology has been recently demonstrated.[30] Like many other compounds in the BTBT family, Ph-BTBT-

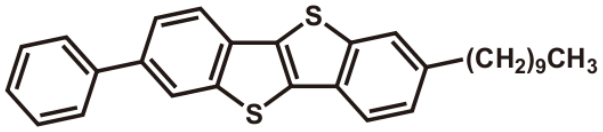

Figure 1: The chemical structure of the mesogenic semiconductor 7-decyl-2-phenyl[1]benzothieno[3,2-*b*][1]benzothiophene (Ph-BTBT-C10).

C10 (see again Fig. 1) does not show a nematic phase, normally required to obtain well aligned monodomains. Instead, layered smectic A and the hexagonally ordered E phases were observed in thin films before crystallization.[22] Record performances of Ph-BTBT-C10 based OFETs were actually obtained not in monodomain, but in polycrystalline solution-processed films and seem to be linked to a thermal treatment that allows the formation, through annealing, of a bilayer crystal rather than a monolayer one inheriting the structure of the smectic phase.[22] The structure of the monolayer nature has also been object of debate between two alternative forms, corresponding to an antiparallel or a nanosegregated model.[31–33]

Theoretical and modelling work on BTBT derivatives has focused more on the transport properties calculation in the crystal phase, rather than in a concomitant exploration of morphologies,[34,35] possibly because of the difficulties inherent to the obtainment of a reliable self-assembled structure at different temperatures.[36] In this context, Yoneya[33] has recently reported on Kinetic Monte Carlo (KMC) calculations of transport, but focusing on the possible monolayer crystal morphologies, which he obtained by relatively short (10 ns)

molecular dynamics (MD) simulations starting from experimental X-ray structures with the bilayer morphology. In the present work we have set ourselves the ambitious task of studying by atomistic MD the self-organization of the Ph-BTBT-C10 smectic phase starting from the isotropic melt in a cooling down sequence, and also in a heating scan starting from the crystal phase. The simulations have been validated against the observed transition temperatures and available X-ray diffraction data. The morphologies obtained from them are eventually employed as an input to KMC simulations based on a hopping model of charge transport, giving a prediction of the charge mobility and especially its temperature dependence across the phases.

Computational Methods

MD simulations of bulk Ph-BTBT-C10 were run at atmospheric pressure and different temperatures (NPT conditions) with the NAMD code[37] using AMBER/GAFF parameters.[38] The torsional potential for the phenyl-BTBT torsion was reparametrized against energy values obtained by constrained geometry optimization at DFT level run with Gaussian09[39] using the PBE0 functional[40] and the cc-pVTZ basis set, following the procedure described elsewhere[41] (see also Fig. S1). Atomic charges needed for the Force Field were calculated with the ESP method[42] at the same level of theory. Simulations were run with three-dimensional periodic boundary conditions employing the smooth particle mesh Ewald method for electrostatics. Parameter and topology files in CHARMM format and a typical NAMD input are provided in the Supporting Information.

Two series of simulations were undertaken, corresponding to cooling and heating sequences. In the first series, we started from a disordered, isotropic liquid configuration of 1000 molecules at 510 K and gradually decreased the temperature to 350 K. In the second series, we started from the experimental crystal structure at room temperature (Cambridge Structural Database entry "ROQSAT"[43]). We built from it a $12 \times 10 \times 2$ su-

percell containing 960 molecules and increased the temperature from 293 K to 498 K, until reaching the isotropic liquid phase. The simulation of this supercell at atmospheric pressure and room temperature provided a first validation of the force field through a satisfactory comparison of simulated cell parameters (a=6.592 Å, b=7.461 Å, c=51.23 Å, α=90°, β=93.55°, γ=90°) with experimental ones (a=6.0471 Å, b=7.7568 Å, c=53.124 Å, α=90°, β=93.135°, γ=90°). All simulations were carried out allowing anisotropic cell expansion; in heating simulations α and γ were fixed to 90°, in accord with the symmetry of Ph-BTBT-C10 crystal cell, while in cooling all angles were kept at 90°, to match the symmetry of liquid and smectic phases.

For both sequences, the preliminary phase diagram was sketched with smaller samples (125 and 120 molecules in cooling and heating, respectively), that were eventually replicated eight times at each temperature to produce larger size initial configurations. After the replication, further equilibration was performed for at least 40 ns, and production runs were conducted for at least 40 ns, checking the stabilization of the values of energy, density, nematic and smectic order parameters.

Zero-field hole mobility estimates were obtained via KMC simulations, with hopping rates described by the semi-classical Marcus formalism on molecular configurations extracted from the MD simulations. The mobility calculations were carried out at six thermodynamic state points, namely 293 and 410 K for the crystalline phase from heating runs, 430, 460, and 490 K for the liquid crystal phase, and 496 K for the isotropic phase, all the latter extracted from cooling runs. Two snapshots per MD simulation, at least 5 ns apart, were included in the KMC simulation in order to assess the variability in the calculated mobilities.

According to the Marcus equation, the rate of electron/hole transfer from a molecule p to a neighboring molecule q is:[7]

$$k_{pq} = \frac{V_{pq}^2}{\hbar}\sqrt{\frac{\pi}{\lambda k_B T}}\exp\left[-\frac{(\Delta\varepsilon_{pq}+\lambda)^2}{4\lambda k_B T}\right]. \quad (1)$$

Its main ingredients are the inter-site orbital couplings V_{pq}, the inter-site energy difference $\Delta\varepsilon_{pq}$=ε_p-ε_q (in the presence of an electric field, there would be an additional contribution from the electrostatic potential at the sites), and the reorganization energy, which is typically considered to be the sum of an inner- and an outer-shell contribution: λ=λ_{in}+λ_{out}. The former was calculated by Nelsen's "four point" approach at the B3LYP/6-311G(d,p) level:[44,45]

$$\lambda_{in} = (E_c^* - E_c) + (E_0^* - E_0) \tag{2}$$

where E_c and E_0 are the energies of a charged and a neutral molecule in the gas phase at their respective equilibrium geometries, whereas E_c^* and E_0^* are the energies of a charged / neutral molecule at the equilibrium geometries of the neutral / charged states. The value λ_{in}=248 meV thus obtained agrees with literature results on Ph-BTBT-C10.[33]

Some of us have shown elsewhere,[46] that a certain degree of ambiguity in the site energies produced by the dimer projection method could be overcome by significantly more expensive calculations on larger molecular clusters, but these were not practically feasible here. In any case, while all the molecules are symmetry-related in the crystal, so that $\Delta\varepsilon_{pq} = 0$ exactly, in the liquid phases, this is only valid on average, and instantaneous fluctuations of nuclear and electronic positions in surrounding molecules could contribute to increasing λ_{out}.[47] In addition, the first-principles estimation of the outer-shell contribution is very challenging,[48,49] if at all possible for a system like ours and it was not attempted here. Recent estimates of its crystal-phase value for BTBT-based molecules are in the range of 20-30 meV, which is indeed negligible compared to the internal contribution.[50] Thus, the outer-shell contribution to the reorganization energy (λ_{out}) was set equal to zero in all KMC simulations. Concerning the energetic disorder (the deviations from zero of $\Delta\varepsilon_{pq}$ that persist on time scales longer than the one for charge hopping, i.e. the picosecond scale), we carried out KMC simulations both with no disorder and in its presence. For the latter case, the site energies were randomly assigned at the beginning of each KMC run, drawing them from a suitable Gaussian distribution. For each thermodynamic state, the standard

deviations were obtained from the distributions of the HOMO orbital energies, extracted from BLYP/6-31G(d) calculations on isolated molecules. The values are of the order of 70 meV in the crystal phase and around 85 meV in the liquid phases (see Table S2 for details). The electrostatic disorder evaluated according to refs.[51,52] is actually very small in the crystal phases (10 meV), confirming that the neglect of site energy disorder is a good approximation in these cases, while the electrostatic disorder is about one order of magnitude larger in the liquid phases (100 meV; see again Table S2 and related text for further calculation details). The effective hole transfer integrals or HOMO-HOMO orbital couplings V_{pq} were computed at the MD geometry via the self-consistent, non-counterpoise variant of the dimer projection method[53,54] at the BLYP/6-31G(d) level, with the ORCA quantum chemistry program, version 4.1.1.[55] Molecular pairs were selected as the ones having at least one atom-atom distance r_{AA} lower than 6 Å. The distance was calculated between any pair of non-hydrogen atoms of the two different molecules, neglecting also aliphatic carbons. We observed that integrals computed at the BLYP/6-31G(d) level, as well as those based on a few other GGA functionals, correlate very well with integrals computed with the B3LYP functional using the same basis set (see Fig. S4). In particular, a linear fit returned a 1.07 scaling factor between B3LYP and BLYP integrals. Further tests involving B3LYP calculations with a larger basis set, *i.e.* 6-311G(d,p), highlighted a significant underestimation of transfer integrals with the smaller basis (see Fig. S5). A linear fit returned in fact a scaling factor of 1.245. This multiplicative factor was used to correct the BLYP/6-31G(d) transfer integrals to values more consistent with B3LYP/6-311G(d,p), prior to rate constants evaluation. A further correction to the orbital couplings was also employed, to include the effect dynamic off-diagonal disorder:[56,57]

$$V_{pq,C}^2 = V_{pq,Q}^2 + s_V^2(r_{AA})\,. \tag{3}$$

Here $V_{pq,Q}$ represents a coupling obtained by the previous quantum chemical procedure

(including the 1.245 rescaling), and $s_V^2(r_{AA})$ is a function of the aforementioned minimum interatomic distance r_{AA}. To derive its values, orbital couplings from all snapshots were collected and binned in 0.2 Å intervals according to the r_{AA} values, and bin-wise variances σ_V^2 computed. The $s_V^2(r_{AA})$ term was fitted over σ_V^2 in the range 0-6 Å (actually, no values were found below 2.8 Å) with a piecewise function combining two exponential decays (see Figs. S6 and S7):

$$s_V^2(r_{AA}) \approx \begin{cases} 3010.9\, e^{-4.45\, r_{AA}}\ \mathrm{eV}^2 & \text{if } r_{AA} \leq 4.2\ \text{Å} \\ 160.8\, e^{-1.37\, r_{AA}}\ \mathrm{eV}^2 & \text{if } r_{AA} > 4.2\ \text{Å}\,. \end{cases} \tag{4}$$

KMC simulations were performed with the Bortz-Kalos-Lebowitz algorithm (BKL)[58] using both the corrected orbital couplings (Eq. 3) and the quantum chemical ones for comparison. Molecules were considered to be frozen over the course of a KMC simulation.

Zero field mobilities were computed from the mean-square displacements (MSD) of the charge carriers along selected directions,[59] typically lying within the herringbone of the crystals or the layers of the smectic phase. According to the Einstein-Smoluchowski relation, the mobility μ along a direction $\mathbf{u}$ is proportional to the charge diffusion coefficient D_e, and is defined as:

$$\mu(\mathbf{u}) \;=\; \frac{eD_e}{k_BT} \;=\; \frac{e}{k_BT} \lim_{t\to\infty} \frac{1}{2t} \left\langle \{[\mathbf{r}(t) - \mathbf{r}(0)] \cdot \mathbf{u}\}^2 \right\rangle \tag{5}$$

where e is the elementary charge and $\mathbf{r}(t)$ is the coordinate of the diffusing charge at time t. The angular brackets indicate an average over 1000 independent KMC simulations, for each of the selected MD snapshots, as well as over all possible time origins. Each simulation lasted in slight excess of 10^7 steps, in order to achieve large MSDs (several hundred times the simulation box lengths). In practice, the infinite time limit in Eq. (5) was evaluated by linear fits of the MSDs over a time range going from 5% to 50% of the total simulation time. As customary, the initial and final sections were excluded from the fits in order to

avoid the erratic, non-diffusive behavior which characterizes the short-time motion of the charge carriers and the statistically poor data at long times. Linearity of MSD vs. time over this interval was verified in each case (see Tables S3-S6).

Results and Discussion

Simulated morphologies

The spontaneous formation and the structure of the thermotropic mesophases of the two Ph-BTBT-C10 samples were first assigned examining the variation with temperature of density and molar enthalpy in the range 410 K–500 K, following both the cooling and heating sequences.

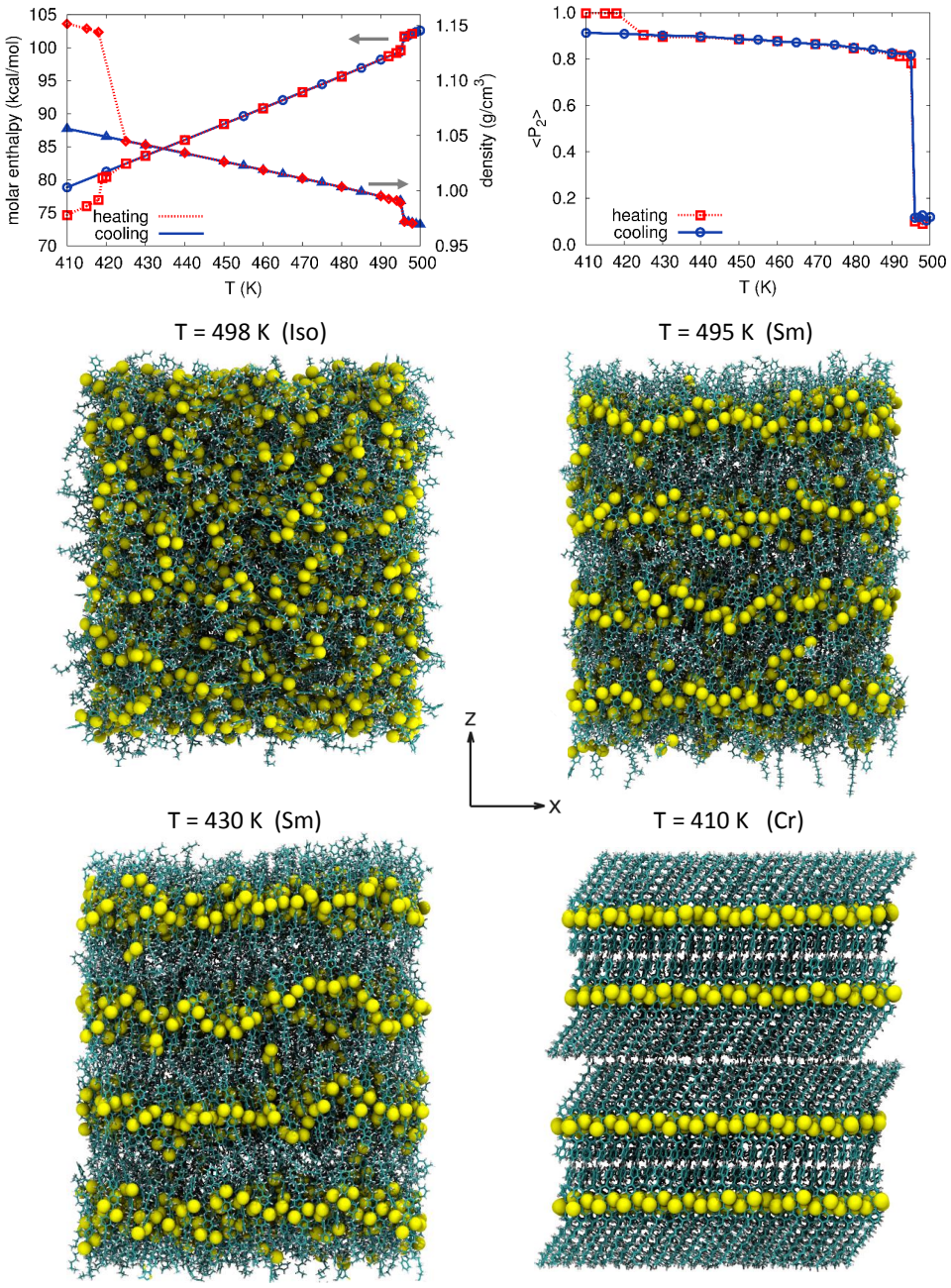

Figure 2: Top: Comparison between cooling vs. heating runs of the average values of physical properties against temperature. On the left: molar enthalpy (squares and circles) and density (triangles and diamonds). On the right: orientational order parameter $\langle P_2 \rangle$ (squares and circles). Middle and bottom: Snapshots of the side view of molecular organization at selected temperatures T=498 K (isotropic, cooling sequence), T=495 K (smectic just below the transition, cooling sequence), T=430 K (low temperature smectic, cooling sequence), T=410 K (crystal, heating sequence). Yellow spheres represent sulfur atoms.

To highlight the mesogenic properties and evaluate the transitions between phases of different orientational order, we examined also the temperature dependence of the second rank orientational order parameter, i.e. the ensemble-averaged second Legendre polynomial $\langle P_2 \rangle = \left\langle \frac{3}{2}\cos^2\beta - \frac{1}{2} \right\rangle$, where β is the angle between the vector connecting the two farthest atoms of the BTBT aromatic core (the “long axis") and the director (the direction of maximum alignment), calculated as described in our previous work.[60]

These profiles are reported in Fig. 2 and they reveal two first order phase transitions, one occurring between 420 and 425 K, the other between 495 and 496 K. The variation of orientational parameter indicates that the latter is an isotropic to ordered phase transition, in excellent agreement with the experimental observation of an isotropic-smectic A transition at 498 K.[22,61]

In this respect, force field reliability is further confirmed by the absence of any observable hysteresis (the predicted transition temperature does not vary from the heating to the cooling sequence) and by the estimated transition enthalpy of 2 kcal/mol (experimental 1.9 kcal/mol[61]). Conversely, a large hysteresis is suggested by the simulation results for the low temperature transition. In fact, no crystallization is observed in the cooling sequence, which was continued down to room temperature without any hints of phase transition, while in the heating one a transition is observed at 419 K, again in excellent agreement with the experimental value of 420.36 K.

To provide an immediate visualisation of the variation with temperature of the molecular organisations obtained, we display in Fig. 2 representative configurations of the phase at T=498 K (isotropic), T=495 K (smectic just below the transition), T=430 K (well ordered smectic) and T=410 K (crystalline close to the melting temperature). The inspection of the MD snapshots is not sufficient to unambiguously determine the nature of the different phases, thus we have investigated the positional order using two particle distribution functions. In particular we have calculated the radial pair distribution $g(r_{12})$, taking the center of mass of each molecule as the reference point.

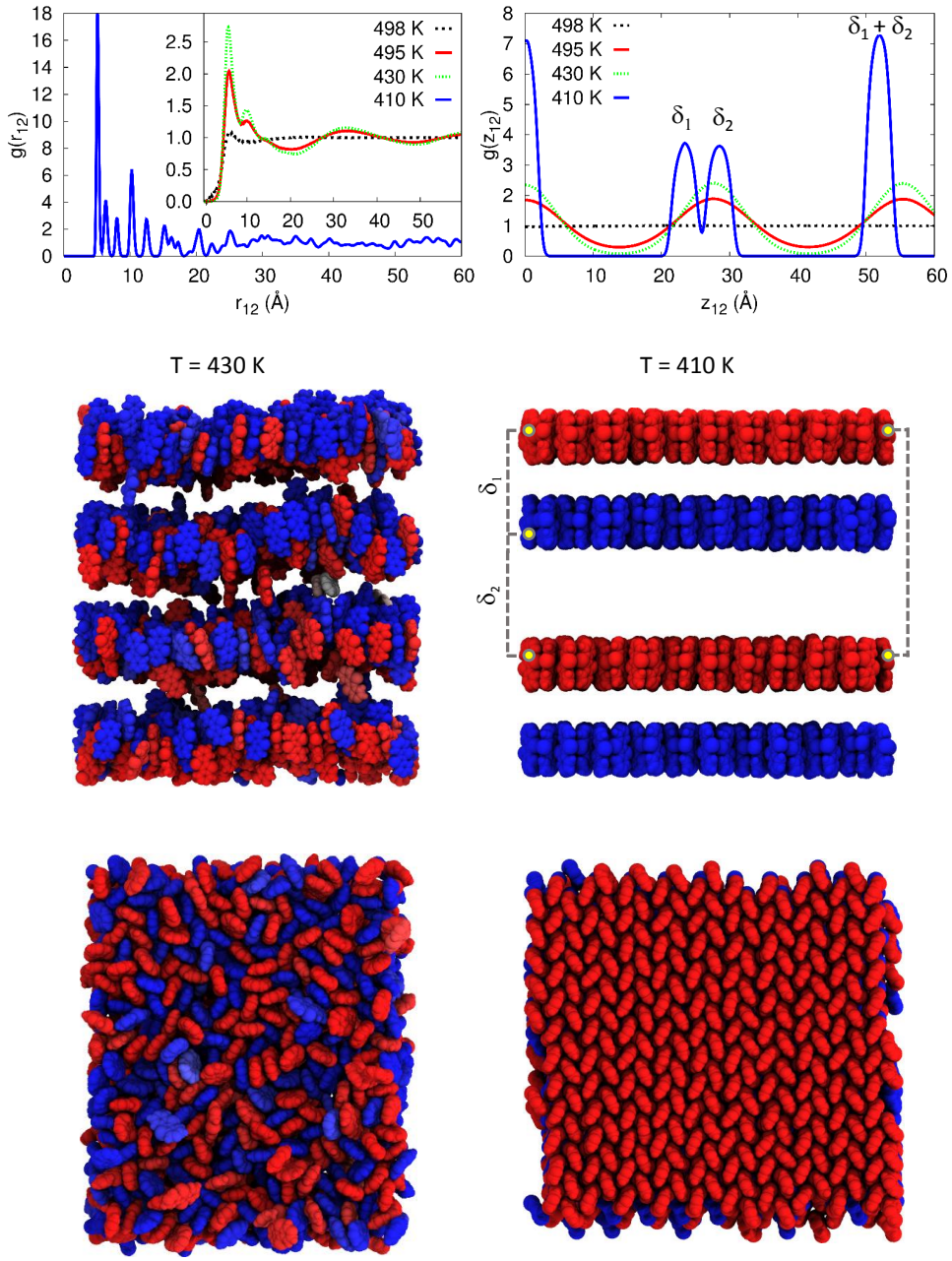

Figure 3: Top: Pair distributions $g(r_{12})$ (left) and $g(z_{12})$ (right) in the isotropic T=498 K and in two smectic temperatures T=495 K and T=430 K taken from the cooling sequence, (shown as an inset for $g(r_{12})$), and in the crystal phase, i.e. T=410 K, heating sequence. Middle and bottom: Snapshots of the molecular organization along x axis (middle plates), and from z axis (bottom plates) of a smectic (T=430 K) and crystal (T=410 K) phases. Here, in order to emphasise the organization in layers, we have rendered only the BTBT cores and we have chosen a color code based on their alignment with respect to z, red if parallel, blue if antiparallel. The yellow circles, connected by the dashed lines in the top right snapshot, represent the centers of mass of the Ph-BTBT-C10 molecules and indicate the origin of the peaks in $g(z_{12})$.

Figure 3 contains the results for the same temperatures illustrated by the MD snapshots. It can be seen that the smectic phase has at long range a liquid–like distribution, characterized by the absence of significant peaks, while two distinct maxima are evident at short separations, indicating a local coordination shell. On the other hand, the crystal at T=410 K shows very sharp peaks at short range (the first corresponds to the four nearest neighbors apparent in Fig. 2-bottom right), and a well defined structure even at long distances. To reveal the presence of layers and to quantify the positional order, we have also calculated the pair distribution function along the layer normal, $g(z_{12})$, where z_{12} is the projection of the intermolecular distance vector $\mathbf{r}$ along the normal to the layer. In smectic phases, $g(z_{12})$ typically presents a periodic behavior and can be expanded in a real Fourier series in terms of harmonic functions. The expansion coefficients are linked to the positional order parameters τ_n, expressing instead the expansion coefficients of the single particle probability distribution $P(z)$ of finding a particle center along the layer normal at a distance z from the average layer position:[62,63]

$$g(z_{12}) \approx 1 + \sum_{n=1}^{n_{max}} {\tau_n}^2 \cos\left(\frac{2\pi n z_{12}}{d}\right), \tag{6}$$

$$\tau_n = \left\langle \cos\left(\frac{2\pi n z}{d}\right)\right\rangle. \tag{7}$$

The numerical procedure employed in the calculation of the τ_n's provides also the value of the layer spacing d. A detailed description of the calculations of the order parameters and of their relation with the positional–orientational distribution function is given elsewhere.[63] The profiles for $g(z_{12})$ at T=430 K and T=495 K (shown in Fig.3, top panel) exhibit a periodic series of diffuse maxima with small differences between them, consistently with the weak temperature dependence obtained for τ_{1-3} (see Fig. 4, left panel). For comparison, in the underlying crystal phase (T=410 K) we observe a different pattern, with alternate peaks that clearly indicate the presence of bilayers formed by two sublayers of molecules oriented in opposite directions in order to optimize their interaction.

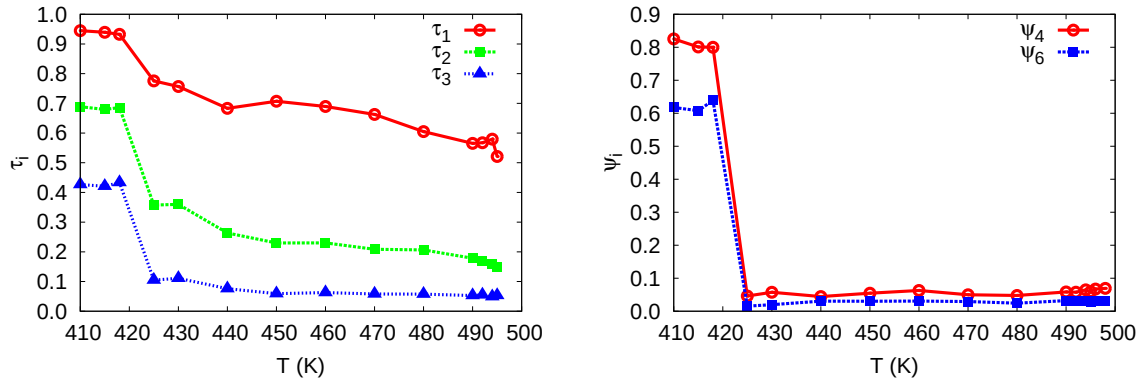

Figure 4: Temperature dependence of the positional order parameters τ_1, τ_2, τ_3 (left) and tetradic and hexatic order parameters ψ_4 and ψ_6 (right) for a system of N=960 Ph-BTBT-C10 molecules in the range 410 - 500 K (heating sequence).

The various types of upright smectics (A, B and E in particular) differ for the absence (smectic A) or the presence (smectic B) of hexatic bond order of the molecular centers surrounding each given molecule.[64,65] The smectic E has, in addition to a possible hexagonal order, also a non uniaxial ordering of the molecular short axes. Other types of in-plane order, e. g. tetragonal, are in principle possible. To quantify the type of order inside the layers of the obtained smectic phases, and accordingly decide on their classification, we have thus calculated both the hexagonal and rectangular global order parameters. These are special cases of the n-th bond order parameter,[65–67] defined as:

$$\langle \psi_n \rangle = \langle \frac{1}{n_k} \sum_{j=1}^{n_k} e^{i n_k \theta_{kj}} \rangle \tag{8}$$

with the sum on j running over the n_k neighbors of molecule k, and θ_{kj} the angle between the interneighbor kj vector and an arbitrary fixed axis and the average is over all molecules k and the simulations. In particular, for $n = 6$ ($n = 4$) we obtain a measure of the hexagonal (rectangular) character of the clustering of centers of mass. Interpreting strictly the neighbors as "nearest neighbors", the two bond orders would appear alternative. However, in a disordered system the definition of neighbors as molecules within a certain cut-off distance is to some extent arbitrary,[65] so we have calculated both ψ_6 and ψ_4 to see which

best describes the observed structures. The profile of the hexatic order parameter ψ_6 vs. T (Fig. 4, right plate) displays in the smectic temperature range values ≈ 0.02, pointing out that our smectic is A rather than B or E. This is confirmed also by the examination of the top view of the T=430 K, displayed in the bottom left panel of Fig. 3, showing extensive positional disorder. In the low temperature crystal phase, the tetragonal order provides instead a better descriptor, as expected for an herringbone packing of the BTBT cores.

Regarding the interlayer distance (see Table S1), we can observe that below 498 K the simulated samples feature a spacing d of about 27.7 Å, which is close to the experimental (X-rays) value of 27–28 Å.[22] The spacing remains constant in the temperature range of existence of the smectic phase. This distance essentially corresponds to a single molecule length and thus to a monolayer structure, as evident from the snapshot of the lateral view of the low temperature smectic (T=430 K) in Fig. 3, middle panel, which shows that BTBT cores within each layer are stacked in an alternating "up" (in red color) and "down" (in blue color) antiparallel fashion. Thus, the simulations indicate that the monolayer antiparallel model is more plausible than the nanosegregated one.[33] For comparison, the crystal phase is characterized by a bilayer structure, with all the BTBT cores packed in a parallel way within each layer. The existence of two sublayers determine the appearance of two separate peaks at distances δ_1 and δ_2 in the $g(z_{12})$ profile (Figure 3), with their sum $\delta_1+\delta_2 \approx 52$ Å coinciding with the crystal cell parameter c and with the main peak of $g(z_{12})$.

It is worth noting that experimentally the monolayer structure of the smectic in Ph-BTBT-C10 can be transformed to a bilayer one, actually the one showing extraordinary mobilities above 10 $cm^2V^{-1}s^{-1}$ by thermal annealing for some minutes of a polycrystalline thin film above the crystal-smectic transition temperature.[32,33] We could not observe this monolayer-bilayer transformation in our MD runs, not unexpectedly given the very different time scales of simulations and experiments. The snapshots in Fig. 3 provide a possible hint as to why it is so difficult to observe the formation of a crystal phase on cooling from the smectic one: in order to form the ordered bilayers, several molecules must either dif-

fuse completely from a layer to an adjacent one (see below), or flip their end-to-end vector by 180°. Both processes are likely to be rather slow in the bulk (much slower than the MD simulation time scale, at least), but they could be promoted in a thin film by a substrate with a higher affinity for either the aliphatic or the aromatic ends of the molecules. To support this hypothesis, we calculated the autocorrelation function of Ph-BTBT-C10 long axis as a function of temperature, which indeed shows that the orientational dynamics becomes extremely slow in the smectic phase at decreasing temperature (see Figure S3).

Given the anisotropic nature of the Ph-BTBT-C10 phases, it is of interest to study the temperature dependence of translational diffusion tensor components D_{ii}, in particular within the smectic phase. From simulations, D_{ii} can be calculated from the mean-square positional displacements using the classic Einstein formula:

$$D_{ii} = \lim_{t\to\infty} \frac{\langle [R_i(0) - R_i(t)]^2 \rangle}{2t} \tag{9}$$

where R_i is the component of the molecular position vector of each molecule along the axis $i = x, y, z$ of the director frame, which has z along the preferred molecular orientation, i.e. along the layer normal. In practice, we assume that the asymptotic long time limit and the diffusive regime are reached for values of $t > 10$ ns, which is adequate, looking at Fig. S2, where linearity is reached much earlier. The parallel and perpendicular diffusion coefficients $D_{||}$ and $D_{\perp}$ correspond to D_{zz} and $(D_{xx} + D_{yy})/2$ respectively, while the isotropic diffusion coefficient D_{iso} was calculated as $(D_{xx} + D_{yy} + D_{zz})/3$. The results are presented in Fig. 5. We see first that, for all smectic temperatures, the diffusion within the layers is faster than that across layers; this trend is not surprising considering the idealized picture of a smectic phase as a set of stacked two dimensional fluid layers, even though counterexamples exist.[63] We also evaluated the activation energies of the parallel and perpendicular diffusions in the smectic range as E_a = 15 and 8.3 kcal/mol respectively, using an Arrhenius fit , i.e. using $D_{iso}(T) = D_0 \exp(-E_a/k_B T)$. Since we are interested in the

possibility of interlayer diffusion in the smectic phase, i.e. diffusion of single molecules between adjacent smectic layers, we evaluated the average time that a molecule takes to travel through a layer spacing d, as $t_d = d^2/D_{||}$, finding values between 50 ns and 350 ns. As we shall see in the next section, these times are considerably larger than the typical residence time of a hole on a given molecule; therefore we expect that molecules which by accident are positioned between two layers (see Fig. 3) could contribute to increase the inter-layer charge mobility.

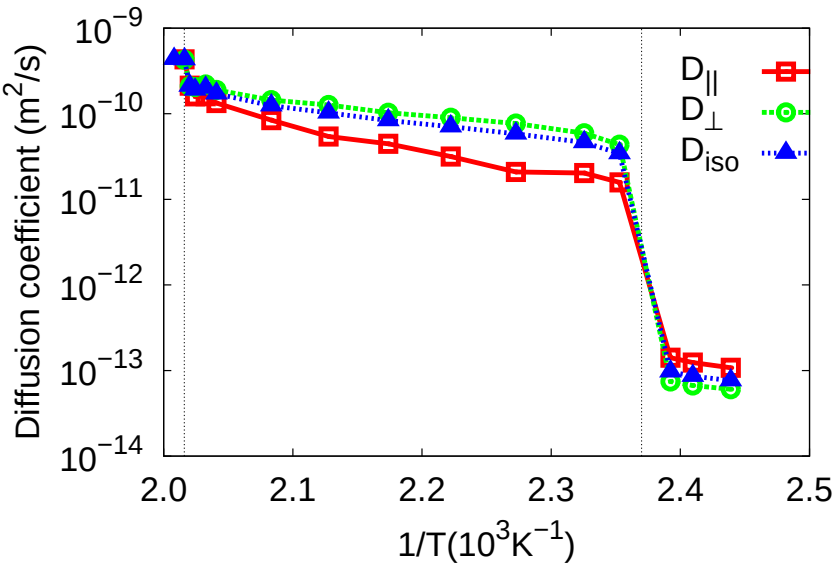

Figure 5: Arrhenius plot of the parallel, perpendicular and isotropic diffusion coefficient, for a system of N=960 Ph-BTBT-C10 molecules in the range 410 - 500 K (heating sequence). The negligible values in the crystal phase are plotted to confirm that molecules do not diffuse at all and to highlight the phase transition to the smectic.

Temperature-dependent charge transport

The zero-field hole mobilities within bulk Ph-BTBT-C10 were computed for each thermodynamic state point by averaging over two thousand independent KMC simulations. In practice, we selected two MD snapshots separated in time by 5 ns for every state and carried out one thousand simulations on each of them, using different starting positions and

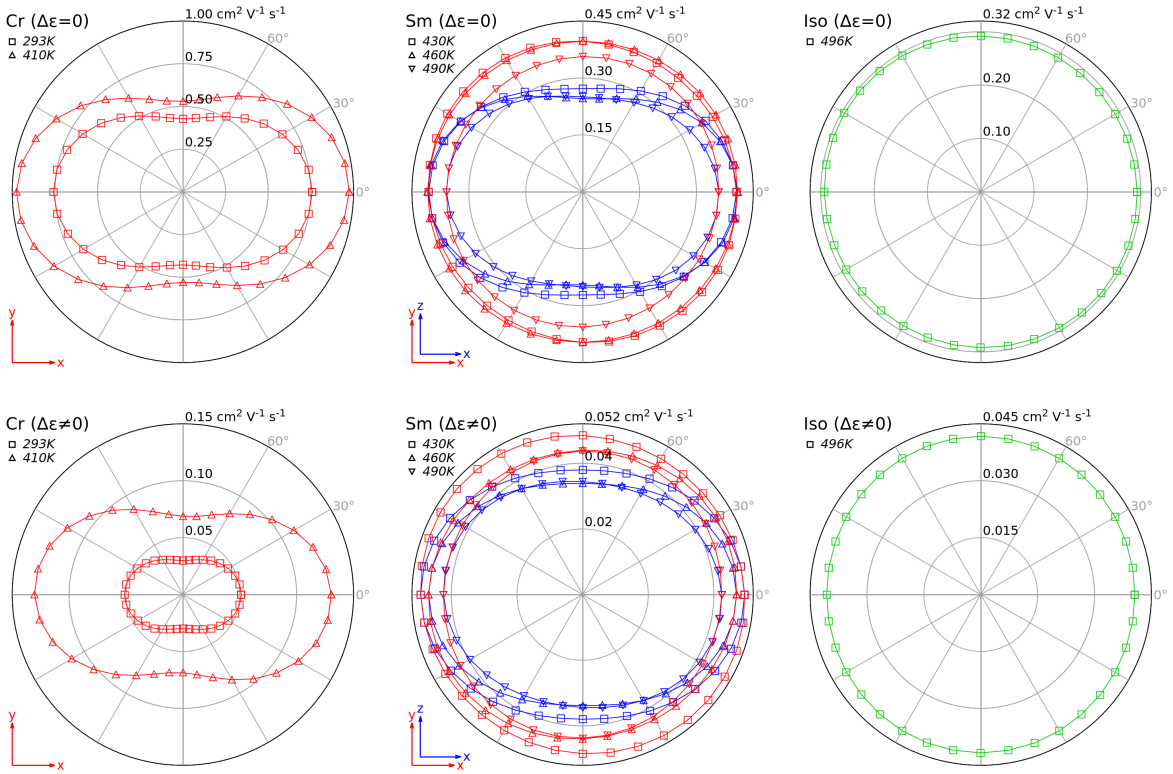

Figure 6: Hole mobilities projected onto relevant planes for the six thermodynamic states, using corrected orbital couplings and zero or non-zero static energetic disorder (upper and lower panels, repectively). The plots have been grouped according to the type of phase: crystalline on the left, smectic in the center and isotropic on the right.

random number seeds. Calculation were performed both without static energetic disorder ($\Delta\epsilon_{pq} = 0$), which is appropriate for the crystal phase, and including it as discussed in the Computational Methods section, an assumption more realistic for the smectic and isotropic phase ($\Delta\epsilon_{pq} \neq 0$).

Fig. 6 collects polar plots of $\mu(\mathbf{u})$, where the unit vector $\mathbf{u}$ lies on selected planes. In the crystals, the layers of herringbone-packed molecules lie on the crystallographic ab plane, which corresponds to the xy Cartesian plane in our simulations. For simplicity, we adopt the same orientation also for the layers within the smectic phase. As such, xy planes in Fig. 6 always correspond to intra-layer charge propagation, whereas z direction represents inter-layer propagation. The mobilities in the isotropic phase have been calculated as the average of projections on three mutually orthogonal planes. A graphical summary of the

temperature dependence of the maximum and minimum hole mobilities is also provided in Figure 7. In view of our previous assessment of the electrostatic energy disorder, below we shall comment in detail the mobilities calculated with $\Delta\epsilon_{pq} = 0$ for the crystals and $\Delta\epsilon_{pq} \neq 0$ for the liquid phases.

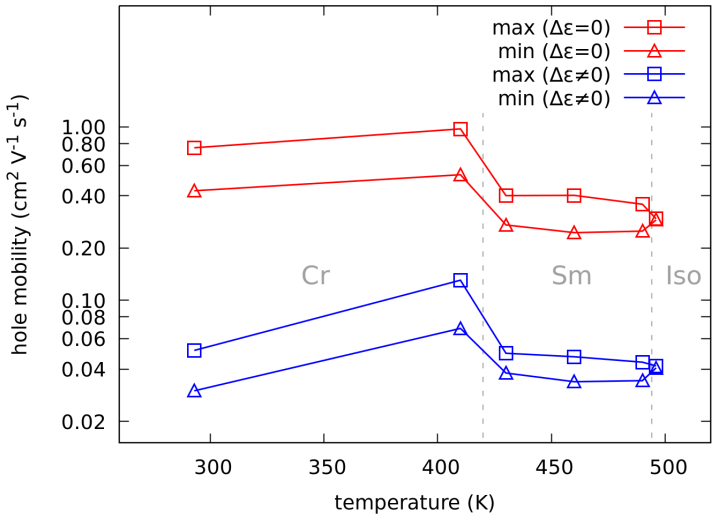

Figure 7: Zero-field hole mobilities calculated both with and without energetic disorder, plotted against simulation temperature. The phases and the transition temperatures are also indicated.

The maximum zero-field hole mobility is achieved along the a axis of the bulk crystal structure. Its calculated value is about 0.8 $cm^2V^{-1}s^{-1}$ at room temperature (293 K), and it increases to 1.0 $cm^2\ V^{-1}s^{-1}$ on increasing the temperature, close to the transition to the smectic phase (410 K). These values are about one order of magnitude smaller than the experimental ones for high quality thin films.[22,68] The hopping model has certainly limitations,[9] and a band mechanism for transport[11,12] should be considered at least for the best performing BTBT materials in crystal phase at very low temperatures (see reference 27 for a comparison between band and hopping transport results, and experiments). However Alkan and Yavuz[50] have recently shown that hopping mechanism is appropriate for BTBTs with long (C8-C12) alkyl chains.[25,50] Moreover, it should not be forgotten that zero-field mobilities are always a lower boundary to experimental ones measured in presence of electric fields.[69] The crystal structure of Ph-BTBT-C10 is characterized by a strong

and sharp segregation into π-conjugated and alkyl layers, which alternate along the z axis. The orbital couplings between molecules on opposite sides of the alkyl layers are close to zero, because of the large distance between the aromatic moieties, which depends in turn on the length of the aliphatic tails. Thus, the alkyl layers are effectively insulating in the crystal phase. The hole transfer network only allows back and forth hops between pairs of head-to-head, monodirectional layers. Although this feature prevents the calculation of hole mobility in the z direction of the crystal, intra-bilayer hopping events are relatively frequent (see below). They are likely to facilitate charge transport also in the xy plane, by providing alternative routes for the carrier to follow in its pursuit of a "least-resistance" pathway.

Hole mobility is rather constant over the whole range of stability of the smectic phase. Without energetic disorder, its intra-layer value settles at about 40-50% of the maximum crystal mobility at room temperature. However, the inclusion of the site energy differences produces a further order-of-magnitude decrease in the hole mobilities, to values of the order of 5×10^{-2} cm^{2}V^{-1}s^{-1}. The smectic phase mobilities are weakly temperature-dependent, as they only diminish slightly in close proximity of the transition to the isotropic phase, around 490 K. As expected on the basis of the structural characterization described previously (see Figs. 3 and 4), $\mu(\mathbf{u})$ is essentially isotropic within the smectic layers, unlike in the crystal phase. Inter-layer propagation is also systematically observed, leading to mobilities that are about two thirds of the corresponding intra-layer ones. Within one smectic layer, the molecules may take either up or down orientations, and this effectively destroys the insulating alkyl layers that characterize the crystals. Indeed charge carrier mobility along the z direction appears to be the result of dynamic positional disorder at the interface between adjacent smectic layers, which can easily be spotted in the structures in Fig.2 at 430 K as well as at 495 K, and is also related to the possibility of molecular diffusion in the parallel direction z (see Fig. 5).

Mobility estimates for the high-temperature isotropic phase are also reported in Fig.

6, averaging at about 0.045 $cm^2V^{-1}s^{-1}$ after the inclusion of energetic disorder. With reference to Fig. 7, the mobilities predicted for the smectic and especially the isotropic phase still seem to be unusually high. The loss of long- and short-range order, which accompanies the transition from the crystal to the smectic and then to the isotropic phase, can in some cases produce a mobility drop of several orders of magnitude, as actually found in other, unrelated liquid crystalline systems.[18,70,71]

Concerning the comparison with experiments, It should be also noted that the temperature dependence of the mobilities measured for differently substituted BTBT materials is far from simple and shows strong voltage and probing technique dependencies.[25,72] Unfortunately, to the best of our knowledge, there are still no published experimental data for the charge carrier mobility within the smectic and isotropic phases of the Ph-BTBT-Cn series, even though room temperature measurements on samples annealed in the smectic phase and abruptly cooled, yielded to mobilities of 0.24 $cm^2V^{-1}s^{-1}$, i. e. a value bracketed by our predictions for the smectic and crystal phase.[73]

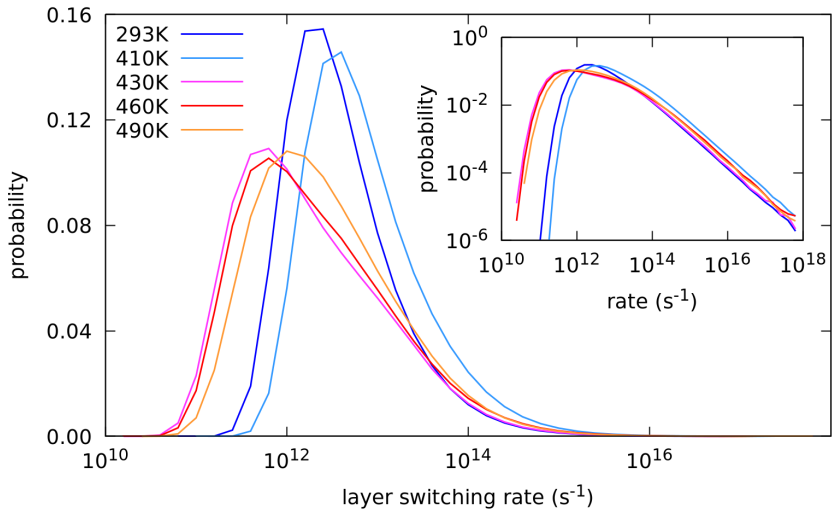

Figure 8: Probability distribution of layer switching rates in the crystalline and smectic states, from the KMC simulations with $\Delta\epsilon_{pq} = 0$.

In order to characterize inter-layer hopping phenomena in greater detail, we monitored the residence time τ_L of carriers on a layer, i.e. the time lapse between one layer change

and the following one. Fig. 8 shows probability distributions for the layer-switching rates (τ_L^{-1}) within the crystalline and smectic phases, in the absense of energetic disorder. While upper bounds in the layer-switching rate probability distributions of the two phases are comparable to one another (see the logarithmic plot in the inset of Fig. 8), the peak values and the lower-bound limits for the smectic phase are nearly one order of magnitude lower than those obtained for the crystalline phase. Once more, we emphasize that despite of the higher frequency of layer-switching events, the charge carriers are confined to bilayers in the crystalline phase. We also point that switching rates above 10^{16} Hz, which appear in the tails of Fig. 8, are not really significant. Due to the definition of hopping time within the BKL kinetic Monte Carlo model as $-\ln(x)/K$, where x is a homogeneously distributed random number taking values between 0 and 1, and K is the sum of the hopping rates relative to all available moves, long simulations such as those discussed are inherently bound to spawn a few instances of extremely short hopping times, up to 10^{-20} s. However unphysical, this represents such a rare occurrence that restraining x to a slightly tighter range would still bear no consequence on the simulated charge carrier mobilities.

Table 1: Likelihood of a layer-switching event, for $\Delta\epsilon_{pq} = 0$.

Temperature	$10^2 \times \mathrm{N}_{inter}/\mathrm{N}_{total}$	$10^2 \times k_{inter}/k_{total}$
293 K	8.06	8.07
410 K	7.95	7.92
430 K	1.26	1.68
460 K	1.31	1.95
490 K	1.40	2.21

Two different estimates of the probabilities of layer-switching events are reported in Table 1 (see also Fig. S6 in the Supporting Information). These estimates depend on the assignment of molecules to layers. This is always straightforward in the crystal phase, but it may be non-trivial and somewhat ambiguous in the liquid crystalline phase, as a few molecules may reside in between the layers. These "bridging sites" are clearly visible in the snapshots of Fig.3. In particular, the N_{inter}/N_{total} ratio represents the number of layer

switching events recorded during a simulation, normalized against the total number of KMC steps. Similarly, k_{inter}/k_{total} is the ratio between two summations of rate constants. Those making up the numerator are associated with spatial displacements of at least 1 nm (a reasonable criterion for inter-layer hopping) in the z direction, while the denominator is the summation of all the rate constants available to the system. It should be noted that a slight discrepancy between the two ratios is to be expected for liquid crystalline phase. While layer switch is a one-step event within neatly packed crystalline systems (hence the much lower difference between the two estimates), the same event between smectic layers requires several steps involving specific percolation pathways. As a result, the rate-based statistics slightly overestimate the layer-switch probabilities in the smectic; but overall the two estimators give consistent results.

The layer switch probability is 5-6 times higher for crystalline systems compared to smectic ones: roughly, a charge carrier performs a layer jump with 8% probability in the crystal phase, and with 1-2% probability in the smectic phase. Each site in the former affords in fact at least four potential transfer paths to the opposite layer, while layer switches in the latter is limited by the presence of bridging sites, and thus constrained to a much smaller pool of possible pathways in the z direction. This intrinsic difference between the smectic and the crystal is confirmed by a further analysis of the overall time spent by the holes on any given site, which is presented in the Supporting Information. The resulting distribution (Figs. S9 and S10) follows a Gaussian statistics in the crystal phase; instead, the distributions are significantly non-Gaussian in the smectic and isotropic phases, with heavy tails at both long and short times.

Conclusions

We have obtained, employing detailed atomistic simulations, the isotropic and smectic morphologies of the high mobility organic semiconductor Ph-BTBT-C10. The isotropic to

smectic liquid crystal phase transition temperature is in excellent agreement (within 2 K) with the experimental one. In our simulations as well as in experiment this transition does not show hysteresis and is well reproduced both in heating and cooling sequences. We observe instead a large hysteresis as shown by the $\langle P_2 \rangle$ orientational order and by the pair distributions in the low temperature region. Indeed we do not observe crystallization in the cooling down sequence, even if the Force Field is validated both by the good agreement with experiment of the isotropic to smectic and by the crystal to smectic in a heating sequence, as well as by the lattice parameters of the simulated crystal structure. We notice that huge hysteresis of over 40 K was also observed experimentally.[22] The hysteresis concerns the solid-smectic transition, but not the actual structure of the smectic phase, which is the same independently of its origin (heating or cooling sequences). This structure is consistent with a smectic A rather than E (hexagonal order is not observed).

As far as hole mobility is concerned, the maximum calculated values are $\mu \approx 0.8$–1 $cm^2V^{-1}s^{-1}$ (crystal at 293 K–410K), ≈0.4 (smectic at 430 K–490 K), while in the isotropic phase $\mu \approx 0.3$ $cm^2V^{-1}s^{-1}$. The absolute values for the crystal are lower, but comparable to the best experimental Field Effect Transistor (FET) ones. The predicted mobility values in the smectic phase are at the upper limit of what typically measured for rod-like materials, and actually similar to the ones measured for Ph-BTBT-C10 polycrystalline films obtained by spin coating a solution at the smectic phase temperature. This is an important result substantiating our methodology, since those films, in absence of annealing, inherit the monolayer structure of the "parent" liquid crystal phase.[22] From the charge transport point of view, this smectic structure turns out to be characterized by an isotropic in-plane mobility and by an out-of-plane mobility remarkably high (about 60% of the out of plane value), a feature which normally is not present in standard crystalline organic semiconductors such as pentacene or rubrene. The fact that predicted charge mobility data in the smectic phase are similar to experiments, while the smectic E phase is not observed, if indicates on one hand a limit of our simulations, also suggests that the formation of an

hexatic smectic E phase is probably not critical to the high semiconductor performance of Ph-BTBT-C10 material, differently from a previously made hypothesis.[22]

Supporting Information

Plots of torsion potential, molecular mean-square displacement, and molecular reorientation autocorrelation function, calculated order parameters, analysis of the calculated orbital couplings, dynamic off-diagonal disorder modeling, corrected orbital coupling distributions, rate constants distributions, site energy static disorder analysis, site occupancies and average residence time distributions, tables of calculated hole diffusivities and corresponding standard deviations (PDF file). Force Field files, one input file, and one configuration file (1000 molecules) for molecular dynamics simulations with NAMD (text files). The Supporting Information is available free of charge on https://pubs.acs.org.

Acknowledgments

We thank MIUR for support through PRIN project 2015XJA9NT "Molecular Organization in Organic Thin Films via Computer Simulation of their Fabrication Processes". C. Z. would also like to thank the Isaac Newton Institute for Mathematical Sciences for support and hospitality within the programme "Mathematical Design of New Materials" (EPSRC Grant Number EP/R014604/1) during the period in which this article was completed.

References

(1) Brédas, J.-L., Marder, S. R., Eds. *The WSPC Reference on Organic Electronics: Organic Semiconductors*; World Scientific: Singapore, 2016.

(2) Samorì, P., Cacialli, F., Eds. *Functional Supramolecular Architectures : for Organic Electronics and Nanotechnology*; Wiley-VCH: Weinheim, 2011.

(3) Da Como, E., De Angelis, F., Snaith, H., Walker, A. B., Eds. *Unconventional Thin Film Photovoltaics*; Royal Society of Chemistry: London, 2016.

(4) Salzmann, I.; Heimel, G.; Oehzelt, M.; Winkler, S.; Koch, N. Molecular electrical doping of organic semiconductors: fundamental mechanisms and emerging dopant design rules. *Acc. Chem. Res.* **2016**, *49*, 370–378.

(5) Skabara, P. J.; Arlin, J.-B.; Geerts, Y. H. Close Encounters of the 3D Kind – Exploiting High Dimensionality in Molecular Semiconductors. *Adv. Mater.* **2013**, *25*, 1948–1954.

(6) Warman, J. M.; de Haas, M. P.; Dicker, G.; Grozema, F. C.; Piris, J.; Debije, M. G. Charge mobilities in organic semiconducting materials determined by Pulse-Radiolysis Time-Resolved Microwave Conductivity: π-Bond-Conjugated Polymers versus $\pi - \pi$-Stacked Discotics. *Chem. Mater.* **2004**, *16*, 4600–4609.

(7) Marcus, R. A. Electron transfer reactions in chemistry. Theory and experiment. *Rev. Mod. Phys.* **1993**, *65*, 599.

(8) Lemaur, V.; Steel, M.; Beljonne, D.; Bredas, J. L.; Cornil, J. Photoinduced charge generation and recombination dynamics in model donor/acceptor pairs for organic solar cell applications: A full quantum-chemical treatment. *J. Amer. Chem. Soc.* **2005**, *127*, 6077–6086.

(9) Coropceanu, V.; Cornil, J.; da Silva Filho, D. A.; Olivier, Y.; Silbey, R.; Brédas, J.-L. Charge transport in organic semiconductors. *Chem. Rev.* **2007**, *107*, 926–952.

(10) Baranovskii, S. D. Mott Lecture: Description of Charge Transport in Disordered Or-

ganic Semiconductors: Analytical Theories and Computer Simulations. *Phys. Status Solidi A* **2018**, *215*, 1–12.

(11) Shuai, Z.; Wang, L.; Li, Q. Evaluation of charge mobility in organic materials: from localized to delocalized descriptions at a first-principles level. *Adv. Mater.* **2011**, *23*, 1145–53.

(12) Troisi, A. Charge transport in high mobility molecular semiconductors: classical models and new theories. *Chem. Soc. Rev.* **2011**, *40*, 2347.

(13) Rühle, V.; Lukyanov, A.; May, F.; Schrader, M.; Vehoff, T.; Kirkpatrick, J.; Baumeier, B.; Andrienko, D. Microscopic Simulations of Charge Transport in Disordered Organic Semiconductors. *J. Chem. Theory Comput.* **2011**, *7*, 3335–3345.

(14) Sokolov, A. N.; Atahan-Evrenk, S.; Mondal, R.; Akkerman, H. B.; Sánchez-Carrera, R. S.; Granados-Focil, S.; Schrier, J.; Mannsfeld, S. C.; Zoombelt, A. P.; Bao, Z.; Aspuru-Guzik, A. From computational discovery to experimental characterization of a high hole mobility organic crystal. *Nat. Commun.* **2011**, *2*, 437.

(15) Watanuki, H.; Mitsuhara, K.; Takizawa, M. Molecular orientation analysis of a C-8-BTBT thin film grown under an external temperature gradient. *e-J. Surf. Sci. Nanotechnol.* **2018**, *16*.

(16) Jiang, L. F.; Liu, J.; Lu, X. Q.; Fu, L. L.; Shi, Y. J.; Zhang, J.; Zhang, X.; Geng, H.; Hu, Y. Y.; Dong, H. L.; Jiang, L.; Yu, J. S.; Hu, W. P. Controllable growth of C-8-BTBT single crystalline microribbon arrays by a limited solvent vapor-assisted crystallization (LSVC) method. *J. Mater. Chem. C* **2018**, *6*, 2419–2423.

(17) Pisula, W.; Zorn, M.; Chang, J. Y.; Müllen, K.; Zentel, R. Liquid crystalline ordering and charge transport in semiconducting materials. *Macromol. Rapid Commun.* **2009**, *30*, 1179–1202.

(18) Hanna, J.; Ohno, A.; Iino, H. Charge carrier transport in liquid crystals. *Thin Solid Films* **2014**, *554*, 58–63.

(19) Zou, C.; Yanahashi, N.; Wu, Y.; Wang, J.; Zhang, C.; Xiong, G.; Yang, H.; Jiang, L.; Ikeda, T. Patterning smectic liquid crystals for OFETs at low temperature. *Adv. Funct. Mater.* **2019**, *29*, 1804838.

(20) Iino, H.; Hanna, J. Availability of liquid crystallinity in solution processing for polycrystalline thin films. *Adv. Mater.* **2011**, *23*, 1748–51.

(21) Minemawari, H.; Yamada, T.; Matsui, H.; Tsutsumi, J.; Haas, S.; Chiba, R.; Kumai, R.; Hasegawa, T. Inkjet printing of single-crystal films. *Nature* **2011**, *475*, 364–7.

(22) Iino, H.; Usui, T.; Hanna, J. Liquid crystals for organic thin-film transistors. *Nat. Commun.* **2015**, *6*.

(23) Chen, H. Y.; Schweicher, G.; Planells, M.; Ryno, S. M.; Broch, K.; White, A. J. P.; Simatos, D.; Little, M.; Jellett, C.; Cryer, S. J.; Marks, A.; Hurhangee, M.; Bredas, J. L.; Sirringhaus, H.; McCulloch, I. Crystal Engineering of dibenzothiophenothieno 3,2-b thiophene (DBTTT) isomers for organic field-effect transistors. *Chem. Mater.* **2018**, *30*, 7587–7592.

(24) Fernandez, A. B.; da Veiga, A. G.; Aliev, A.; Ruzie, C.; Garbay, G.; Chattopadhyay, B.; Kennedy, A. R.; Geerts, Y. H.; Rocco, M. L. M. 1 Benzothieno 3,2-b benzothiophene (BTBT) derivatives: Influence in the molecular orientation and charge delocalization dynamics. *Mater. Chem. Phys.* **2019**, *221*, 295–300.

(25) Wawrzinek, R.; Sobus, J.; Chaudhry, M. U.; Ahmad, V.; Grosjean, A.; Clegg, J. K.; Namdas, E. B.; Lo, S. C. Mobility evaluation of 1 benzothieno 3,2-b 1 benzothiophene derivatives: limitation and impact on charge transport. *ACS Appl. Mater. Interfaces* **2019**, *11*, 3271–3279.

(26) Schweicher, G. et al. Bulky end-capped [1]benzothieno[3,2-b]benzothiophenes: reaching high-mobility organic semiconductors by fine tuning of the crystalline solid-state order. *Adv. Mater.* **2015**, *27*, 3066–3072.

(27) Tsutsui, Y. et al. Unraveling unprecedented charge carrier mobility through structure property relationship of four isomers of didodecyl[1]benzothieno[3,2-b][1]benzothiophene. *Adv. Mater.* **2016**, *28*, 7106–7114.

(28) Ebata, H.; Izawa, T.; Miyazaki, E.; Takimiya, K.; Ikeda, M.; Kuwabara, H.; Yui, T. Highly soluble 1 benzothieno 3,2-b benzothiophene (BTBT) derivatives for high-performance, solution-processed organic field-effect transistors. *J. Amer. Chem. Soc.* **2007**, *129*, 15732–+.

(29) Wu, H.; Iino, H.; Hanna, J. Thermally induced bilayered crystals in a solution-processed polycrystalline thin film of phenylterthiophene-based monoalkyl smectic liquid crystals and their effect on FET mobility. *RSC Adv.* **2017**, *7*, 56586–56593.

(30) Janneck, R.; Nowack, T. S.; De Roose, F.; Ali, H.; Dehaene, W.; Heremans, P.; Genoe, J.; Rolin, C. Integration of highly crystalline C8-BTBT thin-films into simple logic gates and circuits. *Org. Electron.* **2019**, *67*, 64–71.

(31) Miyazawa, T.; Yamamura, Y.; Hishida, M.; Nagatomo, S.; Massalska-Arodz, M.; Saito, K. Revisiting smectic E structure through swollen smectic E phase in binary system of 4-nonyl-4 '-isothiocyanatobiphenyl (9tcb) and n-nonane. *J. Phys. Chem. B* **2013**, *117*, 8293–8299.

(32) Saito, K.; Miyazawa, T.; Fujiwara, A.; Hishida, M.; Saitoh, H.; Massalska-Arodz, M.; Yamamura, Y. Reassessment of structure of smectic phases: Nano-segregation in smectic E phase in 4-n-alkyl-4 '-isothiocyanato-1,1 '-biphenyls. *J. Chem. Phys.* **2013**, *139*.

(33) Yoneya, M. Monolayer crystal structure of the organic semiconductor 7-Decyl-2-phenyl 1 benzothieno 3,2-b 1 benzothiophene. *J. Phys. Chem. C* **2018**, *122*, 22225–22231.

(34) Lemaur, V. et al. Structural and Charge-transport properties of a liquid crystalline α,ω-disubstituted thiophene derivative: a joint experimental and theoretical study. *J. Phys. Chem. C* **2010**, *114*, 4617–4627.

(35) Schrader, M.; Körner, C.; Elschner, C.; Andrienko, D. Charge transport in amorphous and smectic mesophases of dicyanovinyl-substituted oligothiophenes. *J. Mater. Chem.* **2012**, *22*, 22258–22264.

(36) Muccioli, L.; D'Avino, G.; Berardi, R.; Orlandi, S.; Pizzirusso, A.; Ricci, M.; Roscioni, O. M.; Zannoni, C. In *Multiscale Modelling of Organic and Hybrid Photovoltaics*; Beljonne, D., Cornil, J., Eds.; Springer: Berlin, 2014; pp 39–101.

(37) Phillips, J. C.; Braun, R.; Wang, W.; Gumbart, J.; Tajkhorshid, E.; Villa, E.; Chipot, C.; Skeel, R. D.; Kale, L.; Schulten, K. Scalable molecular dynamics with NAMD. *J. Comput. Chem.* **2005**, *26*, 1781–1802.

(38) Wang, J.; Wolf, R. M.; Caldwell, J. W.; Kollman, P. A.; Case, D. A. Development and testing of a general AMBER force field. *J. Comput. Chem.* **2004**, *25*, 1157–1174.

(39) Frisch, M. J.; Trucks, G. W.; Schlegel, H. B.; Scuseria, G. E.; Robb, M. A.; Cheeseman, J. R.; Scalmani, G.; Barone, V.; Mennucci, B.; Petersson, G. A. *Gaussian09 Revision D. 01*; URL: http://www. gaussian. com; Gaussian Inc.: Wallingford CT, 2009.

(40) Adamo, C.; Barone, V. Toward reliable density functional methods without adjustable parameters: The PBE0 model. *J. Chem. Phys.* **1999**, *110*, 6158–6170.

(41) Pizzirusso, A.; Di Pietro, M. E.; De Luca, G.; Celebre, G.; Longeri, M.; Muccioli, L.; Zannoni, C. Order and conformation of biphenyl in cyanobiphenyl liquid crystals: a combined atomistic Molecular Dynamics and H-1 NMR Study. *ChemPhysChem* **2014**, *15*, 1356–1367.

(42) Besler, B. H.; Merz Jr, K. M.; Kollman, P. A. Atomic charges derived from semiempirical methods. *J. Comput. Chem.* **1990**, *11*, 431–439.

(43) Minemawari, H.; Tsutsumi, J.; Inoue, S.; Yamada, T.; Kumai, R.; Hasegawa, T. Crystal structure of asymmetric organic semiconductor 7-decyl-2-phenyl[1]benzothieno[3,2-b][1]benzothiophene. *Appl. Phys Express* **2014**, *7*.

(44) Nelsen, S. F.; Blackstock, S. C.; Kim, Y. Estimation of inner shell Marcus terms for amino nitrogen compounds by molecular orbital calculations. *J. Amer. Chem. Soc.* **1987**, *109*, 677–682.

(45) Stehr, V.; Fink, R. F.; Tafipolski, M.; Deibel, C.; Engels, B. Comparison of different rate constant expressions for the prediction of charge and energy transport in oligoacenes. *Wiley Interdiscip. Rev. Comput. Mol. Sci.* **2016**, *6*, 694–720.

(46) Idé, J.; Fazzi, D.; Casalegno, M.; Meille, S. V.; Raos, G. Electron transport in crystalline PCBM-like fullerene derivatives: a comparative computational study. *J. Mater. Chem. C* **2014**, *2*, 7313–7325.

(47) Tummala, N. R.; Zheng, Z.; Aziz, S. G.; Coropceanu, V.; Brédas, J.-L. Static and dynamic energetic disorders in the C60 , PC61BM, C70 , and PC71BM fullerenes. *J. Phys. Chem. Lett.* **2015**, *6*, 3657–3662.

(48) McMahon, D. P.; Troisi, A. Evaluation of the External Reorganization Energy of Polyacenes. *J. Phys. Chem. Lett.* **2010**, *1*, 941–946.

(49) Ren, H.-S.; Ming, M.-J.; Ma, J.-Y.; Li, X.-Y. Theoretical calculation of reorganization energy for electron self-exchange reaction by constrained density functional theory and constrained equilibrium thermodynamics. *J. Phys. Chem. A* **2013**, *117*, 8017–8025.

(50) Alkan, M.; Yavuz, I. Intrinsic charge-mobility in benzothieno 3,2-b 1 benzothiophene (BTBT) organic semiconductors is enhanced with long alkyl side-chains. *Phys. Chem. Chem. Phys.* **2018**, *20*, 15970–15979.

(51) Tummala, N. R.; Zheng, Z.; Aziz, S. G.; Coropceanu, V.; Brédas, J.-L. Static and Dynamic Energetic Disorders in the C 60 , PC 61 BM, C 70 , and PC 71 BM Fullerenes. *J. Phys. Chem. Lett.* **2015**, *6*, 3657–3662.

(52) D'Avino, G.; Muccioli, L.; Castet, F.; Poelking, C.; Andrienko, D.; Soos, Z. G.; Cornil, J.; Beljonne, D. Electrostatic phenomena in organic semiconductors: Fundamentals and implications for photovoltaics. *J. Phys.: Condens. Matter* **2016**, *28*.

(53) Valeev, E. F.; Coropceanu, V.; da Silva, D. A.; Salman, S.; Bredas, J. L. Effect of electronic polarization on charge-transport parameters in molecular organic semiconductors. *J. Amer. Chem. Soc.* **2006**, *128*, 9882–9886.

(54) Baumeier, B.; Kirkpatrick, J.; Andrienko, D. Density-functional based determination of intermolecular charge transfer properties for large-scale morphologies. *Phys. Chem. Chem. Phys.* **2010**, *12*, 11103–11113.

(55) Neese, F. Software update: the ORCA program system, version 4.0. *WIREs Comput. Mol. Sci.* **2018**, *8*, 1327.

(56) Balabin, I. A.; Onuchic, J. N. Dynamically controlled protein tunneling paths in photosynthetic reaction centers. *Science* **2000**, *290*, 114–117.

(57) Gali, S. M.; D'Avino, G.; Aurel, P.; Han, G. C.; Yi, Y. P.; Papadopoulos, T. A.; Coropceanu, V.; Bredas, J. L.; Hadziioannou, G.; Zannoni, C.; Muccioli, L. Energetic fluctuations in amorphous semiconducting polymers: Impact on charge-carrier mobility. *J. Chem. Phys.* **2017**, *147*.

(58) Bortz, A. B.; Kalos, M. H.; Lebowitz, J. L. A new algorithm for Monte Carlo simulation of Ising spin systems. *J. Comput. Phys.* **1975**, *17*, 10–18.

(59) Di Donato, E.; Fornari, R. P.; Di Motta, S.; Li, Y.; Wang, Z.; Negri, F. n-Type Charge Transport and Mobility of Fluorinated Perylene Bisimide Semiconductors. *J. Phys. Chem. B* **2010**, *114*, 5327–5334.

(60) Tiberio, G.; Muccioli, L.; Berardi, R.; Zannoni, C. Towards in silico liquid crystals. Realistic transition temperatures and physical properties for n-cyanobiphenyls via molecular dynamics simulations. *ChemPhysChem* **2009**, *10*, 125–36.

(61) Inoue, S.; Minemawari, H.; Tsutsumi, J.; Chikamatsu, M.; Yamada, T.; Horiuchi, S.; Tanaka, M.; Kumai, R.; Yoneya, M.; Hasegawa, T. Effects of substituted alkyl chain length on solution-processable layered organic semiconductor crystals. *Chem. Mater.* **2015**, *27*, 3809–3812.

(62) Zannoni, C. In *The Molecular Physics of Liquid Crystals*; Luckhurst, G. R., Gray, G. W., Eds.; Academic Press: London, 1979; pp 51–83.

(63) Palermo, M. F.; Pizzirusso, A.; Muccioli, L.; Zannoni, C. An atomistic description of the nematic and smectic phases of 4-n-octyl-4' cyanobiphenyl (8CB). *J. Chem. Phys.* **2013**, *138*, 204901.

(64) Gray, G. W.; Goodby, J. W. G. *Smectic liquid crystals : textures and structures*; L. Hill: Glasgow, 1984.

(65) Steinhardt, P. J.; Nelson, D. R.; Ronchetti, M. Bond-orientational order in liquids and glasses. *Phys. Rev. B* **1983**, *28*, 784–805.

(66) Brock, J. D.; Aharony, A.; Birgeneau, R. J.; Evans-Lutterodt, K. W.; Litster, J. D.; Horn, P. M.; Stephenson, G. B.; Tajbakhsh, A. R. Orientational and positional order in a tilted hexatic liquid crystal phase. *Phys. Rev. Lett.* **1986**, *57*, 98–101.

(67) Selinger, J. V.; Nelson, D. R. Theory of hexatic-to-hexatic transitions. *Phys. Rev. Lett.* **1988**, *61*, 416–419.

(68) Arai, S.; Inoue, S.; Hamai, T.; Kumai, R.; Hasegawa, T. Semiconductive Single Molecular Bilayers Realized Using Geometrical Frustration. *Adv. Mater.* **2018**, *30*, 1707256.

(69) Baranovskii, S. D. Theoretical description of charge transport in disordered organic semiconductors. *Phys. Status Solidi B* **2014**, *251*, 487–525.

(70) Nakayama, H.; Ozaki, M.; Schmidt, W. F.; Yoshino, K. Measurements of carrier mobility and quantum yield of carrier generation in discotic liquid crystal hexahexyloxytriphenylene by time-of-flight method. *Jpn. J. Appl. Phys.* **1999**, *38*, L1038–L1041.

(71) Wurzbach, I.; Rothe, C.; Bruchlos, K.; Ludwigs, S.; Giesselmann, F. Shear alignment and 2D charge transport of tilted smectic liquid crystalline phases XRD and FET studies. *J. Mat. Chem. C* **2019**, *7*, 2615–2624.

(72) He, D. W.; Qiao, J. S.; Zhang, L. L.; Wang, J. Y.; Lan, T.; Qian, J.; Li, Y.; Shi, Y.; Chai, Y.; Lan, W.; Ono, L. K.; Qi, Y. B.; Xu, J. B.; Ji, W.; Wang, X. R. Ultrahigh mobility and efficient charge injection in monolayer organic thin-film transistors on boron nitride. *Sci. Adv.* **2017**, *3*.

(73) Kim, S.; Kim, A.; Jang, K.-S.; Yoo, S.; Ka, J.-W.; Kim, J.; Yi, M. H.; Won, J. C.; Hong, S.-K.; Kim, Y. H. The effect of thermal annealing on the layered structure of

smectic liquid crystalline organic semiconductor on polyimide gate insulator and its OFET performance. *Synth. Met.* **2016**, *220*, 311 – 317.